ISSN 1070-3632, Russian Journal of General Chemistry, 2015, Vol. 85, No. 5, pp. 1252–1259. © Pleiades Publishing, Ltd., 2015.
Original Russian Text © I.I. Amirov, 2013, published in Rossiiskii Khimicheskii Zhurnal, 2013, Vol. 57, Nos. 3–4, pp. 44–51.

Plasma Chemical Etching of High-Aspect-Ratio Silicon Micro- and Nanostructures

I. I. Amirov

Yaroslavl Branch, Physical Technological Institute Federal State Budgetary Enterprise, Russian Academy of Sciences, ul. Universitetskaya 21, Yaroslavl, 150007 Russia
e-mail: ildamirov@yandex.ru

Received January 1, 2013

Abstract—High-aspect-ratio (HAR) silicon etching of micro-and nanostructures in a time-multiplexed deep etching process (Bosch process) is reviewed, including applications, different technological methods, critical challenges, and main principles of the technologies. HAR silicon etching is an application associated primarily with micro- and nanostructures. This potentially large-scale application requires HAR etching with a high throughput and controllable profile and surface properties. The most significant effects like RIE lag, bowing, stop effect, and profile shape dependence are discussed.

DOI: 10.1134/S10703632150540424

Plasma chemical technologies for etching of silicon micro- and nanostructures are being developed primarily in response to demands of nanoelectronics and micro- and nanosystem technologies [1]. The necessity in deep etching of high-aspect-ratio nanostructures arose, when the size of integrated microcircuit elements had reached the nanometer range (d <100 nm). In the modern plasma technologies for nanoelectronics (element size 20 nm), high-aspect-ratio nanostructures are used for fabrication of nanotransistors [2] and shallow trench isolation [3] and of memory cells with aspect ratios (AR) higher than 100 [4].

High-aspect-ratio etch processes have received the greatest development in micro- and nano-fabrication technologies. For high-rate anisotropic silicon etching, a two-stage deep reactive ion etching (DRIE) process or so-called Bosch process (by the name of the patent-holding company) was developed almost two decades ago [5]. This process allowed, along with high-rate Si bulk etching, etching high-aspect-ratio (HAR) microstructures (AR > 20) [6, 7]. As a result, the technological potential for fabrication of nanoelectronic instruments and devices, such as microactuators and inertial sensors (microgyroscopes and microaccelometers) has enhanced considerably [8–13].

At present the Bosch process is used as the basis for the development of fabrication technologies for micro- and nanostructures with a higher aspect ratio, including 3D micro- and nanocolumns, as well as nanowires, which are applied in nanophotonics [14] and nanotechnologies (fabrication of biosensors [15], microbiochips [16], and solar cells [17]).

The Bosch process combines plasma etching and deposition, due to which highly efficient process parameters are provided (high speed, anisotropicity, selectivity). Moreover, by varying process parameters in a selected way, one can obtain structures with a variable etch profile. This is especially important in nanoelectronics, where micro- and nanostructures of a great variety of shapes are needed.

Three groups of etching processes are recognized, depending on the expected result [9]. The first, the most widespread type, includes the processes of surface microstructuring from different-aspect structures with AR < 20. In this case, the process should be optimized so that to produce smooth and vertical sidewall etched structures. The second group includes Si bulk etching. Such processes are used for through etching of silicon plates with the aim to fabricate 3D integrated circuits [18, 19]. Therewith, the etching rate can reach 50 μm/min. The third group includes the etching processes forming structures with an ultrahigh aspect ratio (AR > 25) [20, 21]. The development of technologies on the basis of these processes is restrained by the fact that a different

negative effects distorting the profile of the resulting structures are still to be overcome [22, 23].

The present review is devoted to the Bosch processes in SF_6/C_4F_8 and SF_6/O_2 plasmas, forming HAR microtrench and microcolumn structures.

Bosch Deep Anisotropic Si Etching Process

The basis for the development of the Bosch process was formed by the research on ion-stimulated anisotropic etching of silicon surfaces. Such processes are applied in the microelectronics technology for a more precise copying of the mask image to deeper laying layers [24]. Initially, anisotropic Si etching processes were performed in a fluorine-containing (SF_6/O_2, SF_6/C_mF_n) radiofrequency capacitively coupled plasma [24, 25]. Such plasmas contain two types of particles, specifically, oxygen atoms or fluorocarbon radicals C_mF_n, which passivate the silicon surface, as well as fluorine atoms which effect etching.

Study of the mechanism of etching in such plasma showed that the anisotropicity of Si etching is associated with the concurrent occurrence of ion-stimulated etching and deposition processes on the Si surface [26–28]. A necessary condition for the anisotropic etching to occur is that the etching rate is strongly dependent on the energy of bombarding ions. The surface is etched along the incident ion flux direction at fairly high ion energies, when the thin $SiOF_x$ or fluorocarbon passivation film on the trench bottom, which can hinder etching, is almost absent. The passivation film is only formed on the trench sidewall which is bombarded by ions at grazing angles (Fig. 1). In the case of etching of structures with a small aspect ratio, the thickness of the fluorocarbon polymer film is a few nanometers, and, therefore, it is usually not taken into account. However, when it comes to HAR structures, processes on trench sidewalls acquire extreme significance because of the accumulation of a fairly thick polymer film on the sidewalls.

If trench bottom and sidewalls are bombarded both by passivating and etching particles simultaneously, the processes that occur on the surface being processed are quite complicated in nature. The competition between etching and passivation slows down both these processes, and this makes HAR trenches difficult to obtain.

At present the most common type of plasma used in the trench etching technologies for nanostructure fabrication is a halogen-containing plasma of a complicated (Cl, Br, N_2, O_2) [2, 5]. However, such plasma is unsuitable for etching of HAR silicon microstructures because of the low rate of the process. The etching rate could only be increased in the Bosch process, where the etching and passivation processes are separated in time.

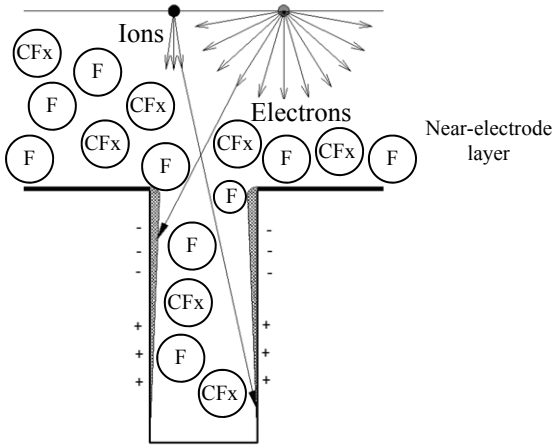

Fig. 1. Motion of charged species toward trench bottom and sidewalls on anisotropic etching in a fluorine-containing plasma.

The Bosch process is realized in a plasma chemical reactor with an inductively coupled RF plasma source [29, 30]. One of the main advantages of such reactors that it allows one to independently control the energy and density of ion current [29]. The reactor comprises two chambers: discharge and reaction. Discharge is ignited in the discharge chamber (a quartz glass) by means of an RF generator (frequency 13.56 MHz). The generated plasma flows from the discharge chamber to a metal reaction chamber. To control the uniformity of etching and increase the density of charged particles, the reaction chamber is placed in magnetic field. The necessary negative bias potential on the electrode which determines the energy of bombarding ions is provided by supplying RF power bias from a separate RF generator.

In the Bosch HAR deep anisotropic silicon etching process, where anisotropic etching is provided by the formation of a passivation film on trench sidewalls, the etching and passivation stages are separated in time. Such separation is realized by alternately supplying the etching (SF_6) and passivating (in the cited works, C_4F_8) reagent fluxes into the plasma chemical reactor. During the passivation stage in the C_4F_8 plasma, a fluorocarbon polymer film is deposited on the trench

bottom and sidewalls. During the subsequent etching stage in the SF_6 plasma the film is rapidly removed from the trench bottom, after which silicon is removed by reacting with fluorine atoms.

The etching–passivation cycle is repeated many times. Each stage lasts a few seconds. During this time sidewalls are etched only slightly. The passivation film on the trench sidewall should persist to prevent sidewall etching. As a result, trench sidewalls have a characteristic notched profile. The balance between etching and passivation is imperative of the Bosch process.

The performance of the Bosch process depends on a variety of factors (pressure, RF power and shift potential, flow rate and composition of the SF_6/C_4F_8 mixture, wafer temperature, relative passivation and etching times), as well as on the process design. The complexity of the Bosch process is associated with the fact that HAR etching involves five concerted processes that occur at the bottom of a trench and at its sidewalls: radical Si etching in the SF_6 plasma, ion-stimulated etching and deposition of a fluorocarbon polymer film on the trench bottom, as well as radical etching and deposition of the film on the sidewall. In view of the fact that the etching process is complex and multiparameter, its simulation becomes a necessary element of research into it. Simulation including all surface reactions resulted in a fair fitting of the experimental data, implying that the mechanism of this process is fairly well understood [31, 32].

For high rate and anisotropicity of Si etching, the following conditions should be fulfilled at the etching stage of the Bosch process. First, the rate of Si etching should be as high as possible. Second, the angular energy distribution of ions should be as narrow as possible. However, these conditions contradict each other. High-rate etching takes place at increased gas pressure and flow rate, when the concentration of fluorine atoms is a maximum is the highest. However, when this takes place, the number of collisions in the near-electrode layer increases, and the angular energy distribution of ions gets wider. The optimal pressure at the etching stage is 4–5 Pa. High-aspect-ratio structures are formed at even lower pressures.

Under the assumption that ion collisions in the near-electrode layer are negligible, the rms deviation of the ion incidence slope angle is given by the equation [33, 34]:

$$\sigma_i = \arctan\sqrt{\frac{kT_i}{kT_i}}, \quad (1)$$

where k is the Boltzmann constant; T_i, thermal energy of ions; and E_i, kinetic energy of ions. At the ion energy of 100 eV (U_{sb} = –80 V) and T_i = 0.04 eV, this angle is 2°.

As follows from Eq. (1), the higher the ion energy, the narrower is the ion energy distribution. However, in this case, the selectivity of etching of the Si/SiO_2 surface decreases. Therefore, to obtain high- and ultrahigh aspect ration microstructures are better prepared using metal masks.

The passivation stage is as important as the etching stage. The passivation parameters that have impact in the etching process parameters (duration, RF shift power, SF_6 and C_4F_8 flow rates and their ratio, and pressure) should ensure that the polymer films grows primarily on the trench sidewall rather than on the trench bottom. To slow down formation of the polymer film on the trench bottom, a definite RF bias power may be supplied on the wafer. This increases the energy of bombarding ions and prevents polymer film formation on the trench bottom and on the mask surface [35]. However, high shift potentials favor faster SiO_2 etching, which adversely affects the selectivity of the process. Moreover, it should be borne in mind that, as the trench depth increases, the ion flux density at the trench bottom decreases [36, 37], and this changes the polymerization conditions. Polymerization can be either enhanced or attenuated, depending on the relative fluxes of ions and radicals.

Fluorocarbon polymer film deposition is an ion-stimulated process, and , therefore, the polymer film is slower deposited on sidewalls, where the ion flux is weaker. The rate of film deposition rate on a plane surface is 6.0 nm/s, whereas the respective value for the sidewall close to the trench top is about an order of magnitude smaller [35]. Evidence for the ion-stimulated deposition mechanism is provided by the shape of the sidewall film (Fig. 2) [38]. Three-minute monitoring of the deposition into deep trenches etched in the Bosch process showed that the film grows along the direction of ion flux incidence, whereas between the deposit build-ups, where the deposition is controlled by the radical flux, the film thickness is much smaller (Fig. 2b). The sidewall film thickness was determined by the angular distribution of ions.

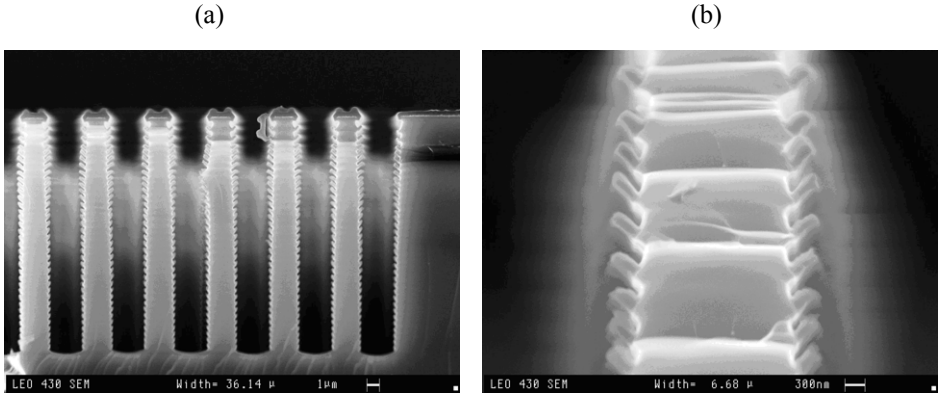

Fig. 2. Fluorocarbon polymer film deposited into (a) deep trenches with crests on their sidewalls and (b) shape of the film on the top of the trench sidewall.

The mechanism of fluorocarbon plasma-enhanced film deposition is still not understood to sufficient detail. As shown more than two decades ago, this process is stimulated by low-energy ion bombardment [39, 40]. It was assumed that under low-energy ion bombardment the fluorocarbon polymer film forms predominantly from CF, CF_2, and CF_3 radicals. The rate of radical polymerization is 5–10 times lower compared to the ion-simulated process. However, later, after it had been established that the surface being processed in itself works as a source of light radicals, researchers started to believe that film formation involves heavy radicals C_xF_y ($x, y > 3$) [41, 42].

Etching of the polymer film in the SF_6 plasma is, too, an ion-stimulated process. Therefore, it is rapidly removed from the trench bottom and slowly removed from sidewalls, where etching is predominantly a radical process. Therewith, one also should account for sidewall etching produced by ions incident at grazing angles. This factor, too, depends on the angular distribution of ions. However, as mentioned above, this function is generally unknown. Therefore, the optimal process parameters, in particular, the durations of the etching and passivation stages, when the rate of microstructure formation on vertical walls is a maximum, are determined experimentally [33, 43].

Formation of Ultrahigh Aspect Ratio Silicon Microstructures

If the etching conditions are invariable over the course of the process, the highest aspect ratio attainable for trenches with vertical walls is 30 [20, 34]. As the trench depth increases, the thickness of the passivation film on the trench sidewalls tends to decrease. As a result, the radical and ion fluxes incident onto the trench bottom and sidewalls also decrease [36, 37], leading to a strong distortion of the micro- and nanostructure profiles, mask underetching, bowing, trench sharpness, and stop etching [20, 34, 43, 44]. A typical profile of thus formed trenches is shown in Fig. 3a. Similar trench profile distortion effects are also observed in a cryogenic SF_6/O_2 plasma Bosch process [45–47].

The angular distribution of ions is a critical factor in HAR trench etching. The formation of barrel-shaped trenches can be explained by the effect of grazing ion bombardment. The angular distribution of ions is responsible for the critical aspect ratio which is defined as the aspect ratio of a trench, the middle point of the bottom of which is reached by ions whose incident angle is equal to the average deviation angle of the ion flux [34].

Trench widening results in that the aspect ratio in fact decreases [34]. The deep mask underetching is associated with decreased thickness of the fluorocarbon polymer film. The fact that the film thickness decreases with increasing trench depth can be explained by a peculiar leading effect. The deeper the trench, the larger is its sidewall surface area and the smaller is the film thickness at a constant fluorocarbon radical flux. Therefore, for HAR structures to form, the passivation conditions should enhance with increasing grove depth. The enhancement should be very essential, because as the trench depth doubles, the trench sidewall surface area increases four times. However, the enhancement of passivation either by prolonging the stage or by increasing the C_4F_8 flow rate in long-term processes (200–500 cycles) can

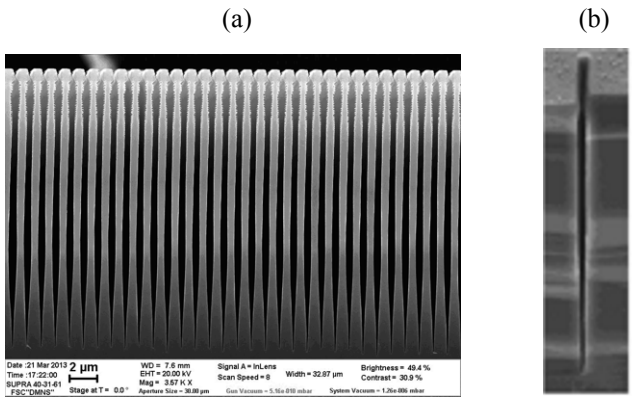

Fig. 3. (a) Typical profile of deep trenches in a Si structure, obtained at invariable etching parameters and (b) profile of a HAR trench obtained at the enhanced passivation stage.

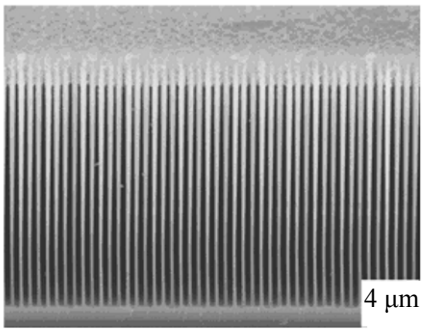

Fig. 4. Fluorocarbon film–coated HAR trenches (AR ≈ 50, width 1 μm) on a Si structure surface, obtained by Bosch etching in a C_4F_8/SF_6 plasma.

results in film accumulation on trench sidewalls near the top. This hinders access of chemically active species depthward the trench, resulting in sharpening of the trench bottom followed by a strong slow-down of the etching process. However, even if passivation is much enhanced, sidewall etching near the trench top still cannot be prevented. This fact can be explained by a nonconformal passivation film deposition on sidewalls [38, 48]. The thickness of a strong sidewall passivation film is nonuniform. Therefore, on prolonged etching, silicon sidewall etching takes place between crests, where the film is the thinnest.

To avoid excess film formation on the trench top, three- and four-stage etching processes were developed [20]. The three-stage process includes the stage of depassivation of the surface being processed in an argon plasma, whereas the four-stage process, one more additional, short stage involving etching of the excess fluorocarbon film. As a result, trenches with ARs higher than 40 could be obtained [20]. However, additional stages slow down the etching process. The excess sidewall film can be removed not in every cycle, but only after 50–100 cycles and additional passivation. In this case, etching slow-down is not so strong, and one can obtain vertical trenches with AR ≈ 50 (Fig. 4).

Higher AR trenches can hardly be fabricated in a fluorocarbon plasma, because the passivation of sidewalls in a C_4F_8 plasma is hindered in view the fact that active species poorly penetrate into the depth of the trench, and film deposition occurs predominantly near the top of the trench. Fluorocarbon films deposited on HAR trench sidewalls are located predominantly on the trench top and eventually encapsulate the latter. The fact that film deposition occurs near the trench top may suggest that the film is charged. The local charging effect is caused by the temperature difference between ions and electrons, and this effect is characteristic of plasma dielectric etching processes [49]. Due to the fact that the charge of the incident electrons and ions is not completely compensated for on the dielectric sidewalls, bombardment of the trench bottom is hindered, and this induces termination of etching (stop effect). However, the charging effect appears to take place if the sidewall film is sufficiently thick. A thin fluorocarbon film is conducting, and its charging should not occur. Experimental evidence for this suggestion was obtained on an example of high-aspect-ratio SiO_2 etching [50, 51].

Thus, for HAR etching one should enhance passivation of the surface being processed and increase the ion bombardment energy. Figure 5 shows trenches with AR > 30, obtained by etching in such conditions. As the energy of ions increases, their angular distribution becomes narrower, and this would favor more vertical sidewalls. The aspect ratio of column microstructures, as defined as the column height-to-width ratio [2], will be about 100. However, it should be noted that such definition is not completely correct, as it does not take account of the physical limitations on the access of etching species. The flux of the etching species in the case of column structures is stronger compared to trenches, and, therefore, the etching depth is former case is higher.

Strictly vertical trenches with AR > 73 could be obtained, when their sidewalls were passivated by oxidation in an oxygen-containing plasma [21]. It

should be noted that even though the high- and ultrahigh-aspect-ratio silicon etching was performed in a Bosch process, the etching rate was fairly low (less than 2 μm/min) in view of aperture limitations. Therewith, no sidewall notches characteristically formed on the trenches fabricated in the cyclic process, are not observed. Such etching can be considered as a quasi-Bosch process. Ultrahigh-aspect ratio structures are difficult to obtain by etching in a continuous mode. Note that cyclic etching failed to provide strictly vertical trenches about, say, 5 μm in width and 500 μm in depth because of process instabilities, sidewall etching, or, vice versa, trench narrowing. All resulting structures with AR > 50 had trench widths of no less than 1 μm.

As mentioned above, by varying passivation and etching conditions one can control the grove profile. Narrowing or widening trenches are formed at different passivation degrees (Fig. 6). Trenches of a more complicated shape, for example, variable-width ones, can be fabricated by varying the passivation degree and the ion energy at the etching stage (Fig. 6a). Simulation also showed that variable-width trenches are formed in a two-stage etching process, in which the first stage forms positively inclined sidewalls and the second stage, vertical walls [52].

Trenches widening bottomward (Fig. 6b) can be fabricated by slightly prolonging the etching stage after structures with a sufficient height have already formed. By varying process parameter in one or another way one can obtain quite diversely shaped structures [53, 54].

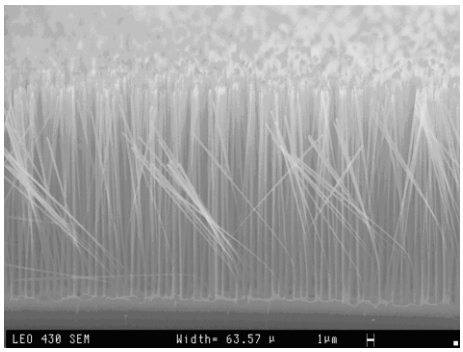

Fig. 5. Ultrahigh-aspect-ratio microcolumn structures 1 μm in width.

Aspect-Dependent and Aspect-Independent Silicon Etching

Wide trenches fabricated by plasma etching are generally deeper compared to narrow ones [55, 56]. The same aperture effect (or aspect-dependent etching) takes place in etching of long microtrenches and microwells (Fig. 7).

The explanation for this effect lies in the fact that as the aspect ratio of the etched structures increases, the limiting stage of the process, specifically, delivery of active species to the bottom of the structures, is slowed down [57]. Simulation of the Bosch etching of deep silicon trenches by fluorine atoms [32] showed that at aspect ratios higher than 12 the etching rate decreases according to the Knudsen transport model [57]. The more probability reaction of fluorine with silicon, the stronger the etching process is slowed down. Thus, if the probability of fluorine reaction with Si is 0.5, the etching rate of trenches with AR 20 decreases more than three times.

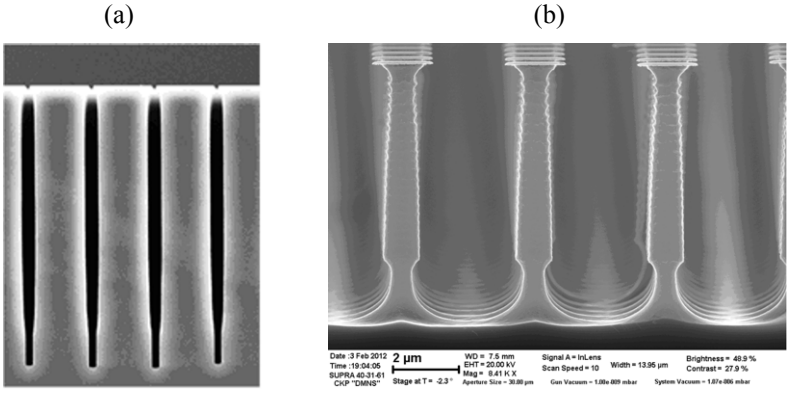

Fig. 6. Changes in trench profile depending on process conditions.

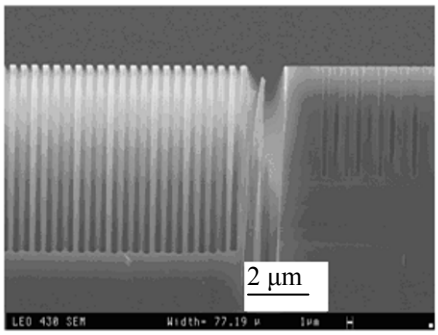

Fig. 7. Microtrenches and microwells 1 μm in width and wide trenches fabricated by HAR etching.

However, in a Bosch process, where the etching stage alternates with the film deposition stage, fluorine transport in not the only limiting factor. Thus, if at the passivation stage a variable-thickness polymer film is formed on the bottom of a wide (with a lower aspect ratio) or narrow trench, removal of such film may become a limiting factor. Therewith, an inverse aperture effect may even be observed.

Analysis of the aspect-dependent Bosch etching process showed that this effect can be suppressed, if the passivation state is much prolonged [58–60]. In this case, the rate of Si etching in wide trenches decreases, while the etching rate in narrow trenches decreases to a much smaller extent. At certain process parameters the etching depths of wide and narrow trenches may prove comparable with each other. Therewith, the sidewalls of wide trenches remain vertical.

Theoretically, such process can be realized to form HAR trenches [58], but in fact trenches of equal heights with AR > 10 could not be obtained. This is explained by the fact that etching after strong passivation results in formation of microneedles on the bottom of a wide trench. As open silicon surface with such needles gets black due to strong light absorption. Research into the mechanism of mucroneedle formation showed that this phenomenon is associated with the micromasking carbon residues formed after etching of the nonuniform-thickness fluorocarbon film on the trench bottom [61, 62]. The same "black silicon" effect is observed in the Bosch process in an SF_6/O_2 plasma [46, 47].

REFERENCES

1. Liberman, M.A. and Lichtenberg, A.J., *Principles of Plasma Discharges and Material Processing*, Hoboken, NJ: Wiley, 2005, 2nd ed., p. 493.
2. Shamiryan, D., Redolfi, A., and Boullart, W., *Microelectron. Eng., 2009, vol. 86. pp. 96–98.*
3. Zhou, H., Ji, X., Srinivasan, S., He, J., et al., *Solid State Technol*., 2013, June, pp. 14–18.
4. Lill, T. and Joubert, O., *Science,* 2008, vol. 319, p. 1050.
5. Laemer, F. and Schilp, A., US Patent 5501893, 1994.
6. Chung, C. K., Lu, H. C., and Jaw, T. H., *Microsyst. Technol*., 2000, vol. 6, pp. 106– 108.
7. Laermer, F. and Urban, A., *Microelectron. Eng.,* 2003, vols. 67–68, pp. 349–55.
8. Fu, L., Miao, J. M., Li, X. X., and Lin, R. M., *Appl. Surf. Sci*., 2001, vol. 177, pp. 78–84.
9. McAuley, S. A., Ashraf, H., Atabo, L., Chambers, A., et al., *J. Phys. D: Appl. Phys*., 2001, vol. 34, pp. 2769–2774.
10. Zhu, Y., Yan, G., Fan, J., Zhou, J., et al., *J. Micromech. Microeng*., 2005, vol. 15, pp. 636–642.
11. Bertz, A., Kuchler, M,, Knofler, R., and Gessner, T., *Sensors Actuators*, 2002, vols. A 97–98, pp. 691–701.
12. Wang, X., Zeng, W., Russo, O.L., and Eisenbraun, E., *J. Vac. Sci. Technol. B,* 2007, vol. 25, pp. 1376–1381.
13. Sarajlic, E., de Boer, M.J., Jansen, H.V., Arnal, N., et al., *Nanotechnology,* 2004, no. 10, pp. 34–40.
14. Hosomi, K., Kikawa, T., Goto, S., Yamada, H., et al., *J. Vac. Sci. Technol*., 2006, vol. B24, pp. 1226–1229.
15. Hanein, Y, Schabmueller, C. G. J., Holman, G., Lucke, P., et al., *J. Micromech. Microeng*.., 2003, vol. 13, pp. S91–S95.
16. Bucaro, M. A., Vasquez, Y, Hatton, B.D., and Aizenberg, J., *ACSnano*, 2012, vol. 6, pp. 6222–6230.
17. Yu, R., Lin, Q., Leung, S-F., and Fan, Z., *Nano Energy*, 2012, vol. 1, pp. 57–72.
18. Topol, A.W., La Tulipe, D.S., Shi Ir.L., et al., *IBM J. Res. Dev*., 2005, vol. 49, pp. 1029–1036.
19. Knickerbocker, J.U., Andry, P.S., Buchwalter, L.P., Deutsch A., et al., *IBM J. Res. Dev.,* 2005, vol. 49, pp. 725–753.
20. Abdolvand, R. and Ayazi, F., *Sensors Actuators A*, 2008, vol. 144, pp. 109–116.
21. Ohara, J., Takeuchi, Y., and Sato, K., *J. Micromech. Microeng*., 2009, vol. 19, p. 095022.
22. Rangelow, I. W., *J. Vac. Sci. Technol. A*, 2003, vol. 21, pp. 1550–1562.
23. Wu, B., Kumar, A., and Pamarthy, S., *J. Appl. Phys*., 2010, vol. 108, p. 051101.
24. *Plasma Processing for VLSI,* Einspruch, N.G. and

Brown, D.M., Eds., New York: Academic, 1985, 1st ed.
25. Pinto, R., Ramanathan, K.V., and Babu, R.S., *J. Electrochem. Soc*., 1987, vol. 134, pp. 165–175.
26. Coburn, J.W., *J. Vac. Sci. Technol. A*, 1994, vol. 12, pp. 1417–1424.
27. Oehrlein, G.S., *Surf. Sci*., 1997, vol. 386, pp. 222–230.
28. Chang, P. and Coburn, J. W., *J. Vac. Sci. Technol. A*, 2003, vol. 21, pp. S145–S151.
29. Cooke, M.J. and Hassali, G., *Plasma Sources Sci. Technol*., 2002, vol. 11, pp. A74–A79.
30. Amirov, I.I., Izyumov, M.O., Morozov, O.V., Kal'nov, V.A., et al., *Mikrosistem. Tekh*., 2004, no. 12, pp. 15–18
31. Zhou, R., Zang, H., Hao, Y., and Wang, Y., *J. Micromech. Microeng*.., 2004, vol. 14, pp. 851–858.
32. Shumilov, A.S. and Amirov, I.I., *Mikroelektronika*, 2007, vol. 36, pp. 295–305.
33. Blauw, M.A., Zijlstra, T., and van der Drifta, E., *J. Vac. Sci. Technol. B*, 2001, vol. 19, p. 2930.
34. Blauw, M.A., Craciun, G., Sloof, W.G., French, P.J., and van der Drift, E., *J. Vac. Sci. Technol. B.,* 2002, vol. 20, pp. 3106–3110.
35. Amirov, I. I. and Alov, N. V., *Khim. Vys. Energ*., 2006, vol. 36, pp. 35–39.
36. Volland, B.E. and Rangelow, I.W., *Microelectron. Eng.,* 2003, vols. 67–68, pp. 338–348.
37. Kokkorisa, G., Boudouvis ,A.G., and Gogolides, E., *J. Vac. Sci. Technol. A*, 2006, vol. 24, pp. 2008–2012.
38. Amirov, I.I., Morozov, O.V., and Izyumov, M.O., *Trudy 4 Mezhdunarodnogo simposiuma po teoreticheskoi i prikladnoi plazmokhimii* (Proc. 4 Int. Symp. on Theoretical and Applied Plasma Chemisty), Ivanovo, 2005, vol. 2, pp. 653–656.
39. Slovetskii, D.I., in *Khimiya plazmy* (Plasma Chemistry), Moscow: Energoatomizdat, 1990, pp. 156–212.
40. Takahashi, K. and Tachibana, K., *J. Appl. Phys*., 2001, vol. 89, pp. 893–899.
41. Kimura, Y, Coburn, J.W., and Graves, D.B., *J. Vac. Sci. Technol*., 2004, vol. A22, pp. 2508–2516.
42. Capps, N. E., Mackie, N. M., and Fisher, E.R., *J. Appl. Phys*., 1998, vol. 84, pp. 4736–4743.
43. Yeom, J., Wu, Y., Selby, J.C., and Shannon, M.A., *J. Vac. Sci. Technol*. B, 2005, vol. 23, pp. 2319–2329.
44. Owen, K.J., van der Elzen, B., Peterson, R.L., and Najafi, K., *Proc. 25th IEEE Int. Conf. on Micro Electro Mechanical Systems (MEMS 2012)*, Paris, France, January 29–February 2, 2012, pp. 251–254.
45. Gomez, S., Belen, R.J., Kiehlbauch, M., and Aydil, E.S., *J. Vac. Sci. Technol. A*, 2004, vol. 22, p. 6064.
46. Jansen, H.V., de Boer, M.J., Unnikrishnan, S., Louwerse, M.C., and Elwenspoek, M., *J. Micromech. Microeng*., 2009, vol. 19, p. 033001.
47. Jansen, H.V, de Boer, M. J, Ma, K., Giron'es, M., et al., *J. Micromech. Microeng.,* 2010, vol. 20, p. 075027.
48. Saraf, M., Goeckner, B., Goodlin, K., Kirmse, L., et al., *Appl. Phys. Lett*., 2011, vol. 98, p. 161502.
49. Ohiwa, T., Kajima, A., Sekine, M., Sakai, I., and Yonemoto, S., *Jpn. J. Appl. Phys*., 1998, vol. 37, pp. 5060–5063.
50. Shimmura, T., Suzuki, Y., Soda, S., Samukawa, S., et al., *J. Vac. Sci. Technol. A*, 2004, vol. 22, pp. 433–436.
51. Ohtake, H., Jinnai, B., Suzuki, Y, Soda, S., et al., *J. Vac. Sci. Technol. A.,* 2006, vol. 24, pp. 2172–2175.
52. Shumilov, S.A., Amirov, I.I., and Lukichev, V.F., *Mikroelektronika*, 2009, vol. 38, pp. 428–435.
53. Kim, B.S., Shin, S., Shin, S.J., Kim, K.M., and Cho, H.H., *Nanoscale Res. Lett*., 2011, vol. 6, pp. 333–339.
54. Jeong, H.E. and Suh, K.Y., *Nano Today*, 2009, no. 4, pp. 335–346.
55. Kiihamaki, J. and Franssila, S., *J. Vac. Sci. Technol. A*, 1999, vol. 17, pp. 2280–2285.
56. Chung, C-K., *J. Micromech. Microeng*.., 2004, vol. 14, pp. 656–662.
57. Coburn, J.W. and Winters, H. F., *Appl. Phys. Lett*., 1989, vol. 55, pp. 2730–2732.
58. Morozov, O.V. and Amirov, I. I., *Mikroelektronika*, 2007, vol. 36, pp. 306–315.
59. Tan, Y., Zhou, R., Zhang, H., Lu, G., and Li, Z., *J. Micromech. Microeng*., 2006, vol. 16, pp. 2570—2579.
60. Lai, S. L., Johnson, D., and Westerman, R., *J. Vac. Sci. Technol. A*, 2006, vol. 24, pp. 1283–1288.
61. Amirov, I.I. and Alov, N.V., *Khim. Vys. Energ*., 2008, vol. 42, pp. 164–168.
62. Amirov, I.I. and Shumilov, A.S., *Khim. Vys. Energ.,* 2008, vol. 42, p. 446.